

A Fast Iterative Method for Removing Impulsive Noise from Sparse Signals

Sahar Sadrizadeh, Nematollah Zarmehi, Ehsan Asadi, Hamidreza Abin, and Farokh Marvasti

Abstract—In this paper, we propose a new method to reconstruct a signal corrupted by noise where both signal and noise are sparse but in different domains. The problem investigated in this paper arises in different applications such as impulsive noise removal from images, audios and videos, decomposition of low-rank and sparse components of matrices, and separation of texts from images. First, we provide a cost function for our problem and then present an iterative method to find its local minimum. The analysis of the algorithm is also provided. As an application of this problem, we apply our algorithm for impulsive noise Salt-and-Pepper noise (SPN) and Random-Valued Impulsive Noise (RVIN) removal from images and compare our results with other notable algorithms in the literature. Furthermore, we apply our algorithm for removing clicks from audio signals. Simulation results show that our algorithms is simple and fast, and it outperforms other state-of-the-art methods in terms of reconstruction quality and/or complexity.

Index Terms—Adaptive thresholding, image denoising, iterative method, impulsive noise, sparse signal.

I. INTRODUCTION

THE problem considered in this paper can be modeled as:

$$\mathbf{Y} = \mathcal{D}^{-1}(\mathbf{X}_0) + \mathbf{N}_0, \quad (1)$$

where the original signal $\mathcal{D}^{-1}(\mathbf{X}_0) \in \mathbb{R}^{m \times n}$ is corrupted additively by sparse noise $\mathbf{N}_0 \in \mathbb{R}^{m \times n}$, and \mathcal{D} is the domain in which the signal is sparse; in other words, the signal and the noise are both sparse but in different domains. We aim to reconstruct the original signal by removing the impulsive noise from the observed signal \mathbf{Y} .

One of the applications of this model is impulsive noise removal from images, videos and audios since these signals are sparse in some domains such as Discrete Cosine Transform (DCT), Wavelet and Contourlet; the impulsive noise is sparse in the image domain. Random missing samples, SPN noise and RVIN (common types of sparse noise) are common phenomenon in image processing, audio and video transition [1]–[3], and data transition over noisy communication channels [4], [5] such as underwater acoustic channels and power line channels. Additionally, in dictionary learning problems where impulsive noise exists [6], [7] (such as random missing samples when no side information about the location of missing samples is available) the problem can be modeled by equation (1). The model stated in (1) also arises in low-rank and sparse matrix decomposition since the singular values of a low-rank matrices are sparse. [8], [9]. Another application of our model

is separation of text from images since the text is sparse in the space domain while the image is sparse in the DCT domain.

The algorithms related to the impulsive noise removal can be divided into two general categories:

In the first category, methods first detect the position of the corrupted samples, i.e., the position of the impulsive noise, and then restore them from other clean samples. In the case of SPN, most of the research are from this category and usually result in a better reconstruction since they first find the mask matrix with which the signal is corrupted [2], [10]–[15]. These methods have two drawbacks: When the original signal is corrupted by RVIN, the detection of noisy pixels becomes very challenging. In addition, all these methods utilize the structure of the audio and image signals (mainly their low-pass characteristic) to detect the location of corrupted pixels and hence they are not applicable to signals other than audio and image signals. As examples of this category, inpainting of audio signals corrupted by impulsive noise is considered in [10]. It is assumed that the location of the distorted data is known and the audio signal is reconstructed through sparse recovery techniques. In [2], noisy pixels are detected through an impulse detector and the image is restored by applying a weighted-average filter. The authors of [11] present a two-step algorithm. In the first step the noisy pixels are detected by Support Vector Machine (SVM) classification, and then they are restored by applying an adaptive fuzzy filter.

The second category consists of methods which detect and restore the noisy samples simultaneously [1], [16]–[20]. The method presented in this paper falls into this category and we compare our results with other algorithms of this class. Examples of this category are as follows: In [16], the Adaptive Median Filter (AMF) is introduced for impulsive noise removal from images. In this algorithm, the window size of the median filter is adjusted according to the impulsive noise density. An Adaptive Median Filter which utilizes the Center-Weighted median (ACWMF) is introduced in [21], and unlike other median-based filters, it performs well in the presence of RVIN. In [22], the Weighted Encoding with Sparse Nonlocal Regularization method (WESNR) is introduced which integrates a soft impulse detection and sparse non-local prior to remove mixed noise from images. The authors of [17] present a method based on Bayesian inference for impulsive noise removal from audio signals. For restoring images corrupted by impulsive noise, a method is suggested in [18] which utilizes particle swarm optimization and fuzzy filtering. The Structure-Adaptive Fuzzy Estimation (SAFE) algorithm is introduced in [20], in which RVIN is removed via Gaussian Maximum Likelihood Estimation. The structure information of the image is incorporated into this algorithm

Author are with the Advanced Communication Research Institute (ACRI), Electrical Engineering Department, Sharif University of Technology, Tehran, Iran (email: ss.sadrizadeh@ee.sharif.edu; zarmehi_n@ee.sharif.edu; ea460@cam.ac.uk; hamidreza.abin@ee.sharif.edu; marvasti@sharif.edu). E. Asadi is currently pursuing PhD degree at the University of Cambridge

as the fuzziness metrics in the form of point reliability and structure similarity. The Annihilating filter-based Low-Rank Hankel Matrix Approach (ALOHA) is proposed in [23]. This method models the impulsive noise as a sparse component, and the underlying image is modeled as a low-rank Hankel structured matrix.

In this paper, a new iterative method is proposed which is applicable to 1-D and 2-D (even higher dimensions) sparse signals. Our algorithm can reconstruct signals which are corrupted by any type of sparse noise such as SPN and RVIN, by contrast to most of the other methods which are applicable to one of these noises. Moreover, the noisy samples are not detecting beforehand. Our method reconstructs both signal and noise iteratively by thresholding them in their corresponding sparse domains and projecting them onto the set imposed by (1). The contributions of this paper are summarized as follows:

1) In this paper, we propose a general framework for impulsive noise removal. The only assumption about the noise and signal is their sparsity in different domains. Therefore, the proposed algorithm can easily be applied to various applications (any dimension) with different noise models. To the best of our knowledge, this is one of the few works with this generality.

2) Since the proposed model (1) is non-convex, we presented an iterative algorithm called Iterative Double Thresholding (IDT) to approximate the solution. The capability of our algorithm is verified analytically and experimentally.

3) By proposing some modifications, a fast method is obtained for impulsive noise removal from images and audios.

The rest of this paper is organized as follows. In Section II, first, a cost function is introduced that generates our algorithm through optimization and then it is analysed. The simulation results are discussed in Section III with comparisons to other methods in the literature. Finally, the paper is concluded in Section IV.

II. THE PROPOSED METHOD

In this section, we illustrate the proposed scheme for removing sparse noise from sparse signal. Then we analyse our algorithm and present some modifications to tailor our applications.

A. Iterative Double Thresholding Algorithm

As mentioned in the introduction, we are considering the problem of reconstructing a signal which is sparse in some domain from its noisy observation; the noise is also assumed to be sparse in the observation domain. As an example of (1), the transformation \mathcal{D} , the original signal and the noise can be the 2-dimensional DCT, an image and impulsive noise, respectively. Therefore, the problem becomes impulsive noise removal from images.

We can consider this problem from another view: we have an overcomplete dictionary (by concatenating matrix representation of the \mathcal{D} transform and the identity matrix), and our goal is to find the sparsest representation of the matrix \mathbf{Y} [24].

For an observed matrix \mathbf{Y} , there may exist infinite numbers of 2-tuples (\mathbf{X}, \mathbf{N}) that satisfy (1), but we are looking for the sparsest pair, that is, the pair with the minimum total number of non-zero entries. This specific 2-tuple is the minimizer of the following optimization problem:

$$\begin{aligned} \underset{(\mathbf{X}, \mathbf{N})}{\operatorname{argmin}} \quad & \|\operatorname{vec}(\mathbf{X})\|_0 + \|\operatorname{vec}(\mathbf{N})\|_0, \\ \text{s.t.} \quad & (\mathbf{X}, \mathbf{N}) \in W, \end{aligned} \quad (2)$$

where $\|\operatorname{vec}(\cdot)\|_0$ represents the L_0 semi-norm of the vectorization of the input matrix, and the set W contains all the (\mathbf{X}, \mathbf{N}) for which (1) holds:

$$W \triangleq \{(\mathbf{X}, \mathbf{N}) | \mathbf{Y} = \mathcal{D}^{-1}(\mathbf{X}) + \mathbf{N}\}; \quad (3)$$

If for the parameters of our problem, the solution of (1) is unique, we can easily conclude that the desired pair $(\mathbf{X}_0, \mathbf{N}_0)$ is the sparsest member of W . We will discuss the uniqueness of the solution later in this section.

This optimization problem (2) is non-convex and NP-hard; hence we present an alternative optimization problem for finding the sparsest member of W . Consider the following function:

$$\begin{aligned} f_\lambda(\mathbf{X}, \mathbf{N}, \mathbf{T}_1, \mathbf{T}_2) \triangleq & \|(\mathbf{1} - \mathbf{T}_1) \odot \mathbf{X}\|_F^2 + \|(\mathbf{1} - \mathbf{T}_2) \odot \mathbf{N}\|_F^2 \\ & + \lambda(\|\operatorname{vec}(\mathbf{T}_1)\|_1 + \|\operatorname{vec}(\mathbf{T}_2)\|_1), \end{aligned} \quad (4)$$

where $(\mathbf{X}, \mathbf{N}) \in W$, $\mathbf{T}_1, \mathbf{T}_2$ are binary matrices, and $\mathbf{1}$ is a matrix of all ones. The sign \odot represents the Hadamard (entry-wise) product of matrices, and $\|\operatorname{vec}(\cdot)\|_1$ denotes the entry-wise L_1 norm (or the L_1 norm of the vectorization) of the input matrix. We will prove later in this section that for small enough values of λ , the minimizer of the following optimization problem is the sparsest member of W , i.e., the solution of (2):

$$\begin{aligned} \underset{(\mathbf{X}, \mathbf{N}), (\mathbf{T}_1, \mathbf{T}_2)}{\operatorname{argmin}} \quad & f_\lambda(\mathbf{X}, \mathbf{N}, \mathbf{T}_1, \mathbf{T}_2). \\ \text{s.t.} \quad & (\mathbf{X}, \mathbf{N}) \in W. \end{aligned} \quad (5)$$

In the first two terms of the cost function, $\mathbf{1} - \mathbf{T}_1, \mathbf{1} - \mathbf{T}_2$ equal the complement of the binary matrices $\mathbf{T}_1, \mathbf{T}_2$, respectively, and thus these two terms compute the sum of squares of the elements of (\mathbf{X}, \mathbf{N}) which are outside the supports $\mathbf{T}_1, \mathbf{T}_2$. The last two terms of the cost function calculate the total number of non-zero entries of $\mathbf{T}_1, \mathbf{T}_2$. Therefore, we are looking for two binary matrices $\mathbf{T}_1, \mathbf{T}_2$ with minimum total number of non-zero entries which are closest to the support (location of non-zero entries) of the two matrices $(\mathbf{X}, \mathbf{N}) \in W$. The parameter λ balances the weight of the two parts of the cost function. It is worth mentioning that this function is convex *w.r.t* (\mathbf{X}, \mathbf{N}) when $(\mathbf{T}_1, \mathbf{T}_2)$ are fixed since the feasible region is a convex set, and the objective function is a quadratic function of (\mathbf{X}, \mathbf{N}) .

Now we present our algorithm for finding the minimizer of (5). The pseudocode of the IDT algorithm is illustrated in Algorithm 1.

As it will be proved in the next subsection, we are looking for the minimizer of f_λ for small enough value of λ . However,

Algorithm 1 IDT

```

1: Input:
2:   Observed matrix:  $\mathbf{Y} \in \mathbb{R}^{m \times n}$ 
3:   Maximum number of iterations of the outer loop:  $K$ 
4:   Decreasing sequence:  $\mathbf{th} \in \mathbb{R}^K$ 
5:   Stopping threshold of the inner loop:  $\delta$ 
6: Output:
7:   Recovered estimate of the signal:  $\hat{\mathbf{X}}$ 
8:   Recovered estimate of the noise:  $\hat{\mathbf{N}}$ 
9: procedure
10:   $\hat{\mathbf{X}} \leftarrow \mathcal{D}(\mathbf{Y}), \hat{\mathbf{N}} \leftarrow \mathbf{0}$ 
11:  for  $k = 1 : K$  do
12:     $\mathbf{X}^0 \leftarrow \hat{\mathbf{X}}, \mathbf{N}^0 \leftarrow \hat{\mathbf{N}}, l \leftarrow 0$ 
13:     $\sqrt{\lambda} \leftarrow \mathbf{th}_k$ 
14:    while  $e > \delta$  do
15:       $\mathbf{X}^{l+1} \leftarrow \text{threshold}(|\mathbf{X}_{i,j}^l|_{i=1,j=1}^{m,n}, \sqrt{\lambda})$ 
16:       $\mathbf{N}^{l+1} \leftarrow \text{threshold}(|\mathbf{N}_{i,j}^l|_{i=1,j=1}^{m,n}, \sqrt{\lambda})$ 
17:       $\mathbf{X}^{l+1} \leftarrow 0.5 (\mathbf{X}^{l+1} + \mathcal{D}(\mathbf{Y} - \mathbf{N}^{l+1}))$ 
18:       $\mathbf{N}^{l+1} \leftarrow 0.5 (-\mathcal{D}^{-1}(\mathbf{X}^{l+1}) + \mathbf{Y} + \mathbf{N}^{l+1})$ 
19:       $e \leftarrow \|\mathbf{N}^{l+1} - \mathbf{N}^l\|_F$ 
20:       $l \leftarrow l + 1$ 
21:    end while
22:     $\hat{\mathbf{X}} \leftarrow \mathbf{X}^l$ 
23:     $\hat{\mathbf{N}} \leftarrow \mathbf{N}^l$ 
24:  end for
25:  return  $\hat{\mathbf{X}}, \hat{\mathbf{N}}$ 
26: end procedure

```

the cost function has many local minimums in this case. Therefore, making use of warm start is necessary. We start with a large λ and iteratively minimize the cost function; then this estimation will be used as an initial guess for the next optimization with lower λ . It is worth mentioning that as λ goes to infinity, the optimization problem becomes convex since the last two terms of the cost function are forced to become zero, and thus $(\mathbf{T}_1, \mathbf{T}_2)$ are all zero matrices. Therefore, our optimization problem reduces to the following one, which is convex:

$$\begin{aligned} \underset{(\mathbf{X}, \mathbf{N})}{\operatorname{argmin}} \quad & \|\mathbf{X}\|_F^2 + \|\mathbf{N}\|_F^2. \\ \text{s.t.} \quad & (\mathbf{X}, \mathbf{N}) \in W. \end{aligned} \quad (6)$$

We initialize the algorithm for a large value of λ in line 10. For a specific value of λ , in order to minimize f_λ , we will alternatively minimize the cost function *w.r.t* $(\mathbf{T}_1, \mathbf{T}_2)$ and (\mathbf{X}, \mathbf{N}) , then we project the resultant minimizers onto the set W so that the constraint of the optimization problem is satisfied.

For a fixed value of λ (in the inner loop of the algorithm), let \mathbf{X}^l and \mathbf{N}^l denote the recovered signal and noise after l iterations. In the $(\mathbf{T}_1, \mathbf{T}_2)$ -minimization step, the minimizers can be found by thresholding (\mathbf{X}, \mathbf{N}) of the previous iteration:

$$\begin{aligned} (\hat{\mathbf{T}}_1)_{i,j} &= \begin{cases} 0, & (\mathbf{X}^l)_{i,j} < \sqrt{\lambda} \\ 1, & (\mathbf{X}^l)_{i,j} \geq \sqrt{\lambda} \end{cases}, \\ (\hat{\mathbf{T}}_2)_{i,j} &= \begin{cases} 0, & (\mathbf{N}^l)_{i,j} < \sqrt{\lambda} \\ 1, & (\mathbf{N}^l)_{i,j} \geq \sqrt{\lambda} \end{cases}, \end{aligned} \quad (7)$$

where $(\cdot)_{i,j}$ is the element of the matrix at the intersection of the i -th row and the j -th column.

In the (\mathbf{X}, \mathbf{N}) -minimization step, a new pair of \mathbf{X}^{l+1} and \mathbf{N}^{l+1} (which is not necessarily in W) is attained by considering $(\hat{\mathbf{T}}_1, \hat{\mathbf{T}}_2)$ to be their respective supports as follows:

$$\mathbf{X}^{l+1} = \hat{\mathbf{T}}_1 \odot \mathbf{X}^{l+1}, \quad \mathbf{N}^{l+1} = \hat{\mathbf{T}}_2 \odot \mathbf{N}^{l+1}. \quad (8)$$

The insertion of (7) in (8) is equivalent to thresholding the entries of \mathbf{X}^l and \mathbf{N}^l by $\sqrt{\lambda}$. This is done in the lines 15 and 16 of Algorithm 1, where $\text{threshold}(|\mathbf{X}_{i,j}^l|_{i=1,j=1}^{m,n}, th)$ represents thresholding the entries of matrix \mathbf{X} based on their absolute values with regard to the threshold level of th .

Now we have to project this pair onto the set W so that the constraint of the optimization problem (5) is met. We will use the following lemma and find the projection of $(\mathbf{X}^{l+1}, \mathbf{N}^{l+1})$ on the set W .

Lemma 1. *The projection of an arbitrary pair (\mathbf{X}, \mathbf{N}) onto the set W defined by (3) is*

$$\begin{cases} \hat{\mathbf{X}} = 0.5 (\mathbf{X} + \mathcal{D}(\mathbf{Y} - \mathbf{N})) \\ \hat{\mathbf{N}} = 0.5 (-\mathcal{D}^{-1}(\mathbf{X}) + \mathbf{Y} + \mathbf{N}) \end{cases}. \quad (9)$$

Proof: See Appendix A. ■

The process of projection (9) is carried out in lines 17 and 18 of Algorithm 1.

The procedure explained above is continued iteratively until the difference between two consecutive estimation $\|\mathbf{N}^{l+1} - \mathbf{N}^l\|_F$ is less than a threshold. Then λ is decreased (outer loop of the algorithm) and the minimizer of the new f_λ is found in the same manner.

From another point of view, our algorithm gradually picks up the main components of the signal and noise. By decreasing parameter λ , i.e., decreasing the threshold level, we are increasing the support size of the estimated signal and noise.

B. Algorithm Analysis

As discussed at the beginning of this section, the proposed algorithm works if we could prove:

1) The solution of the optimization problems (2) and (5) are the same.

2) Under certain conditions, the sparse solution of (1) is unique.

We will investigate these two problems in Theorem 1 and Theorem 2, respectively.

We define ε as follows: For a fixed pair of binary matrices $(\mathbf{T}_1, \mathbf{T}_2)$, the minimizers of f_λ are denoted by $(\mathbf{X}^*, \mathbf{N}^*)$ (which are computed in the algorithm by thresholding and projecting). Since the total number of binary matrices $(\mathbf{T}_1, \mathbf{T}_2)$ is finite, there exists only finite numbers of 4-tuples $(\mathbf{X}^{*i}, \mathbf{N}^{*i}, \mathbf{T}_1^i, \mathbf{T}_2^i)$, which are distinguished by superscript i . We are looking for the 4-tuple for which f_λ is minimum. The

minimum non-zero value of $\|(\mathbf{1} - \mathbf{T}_1) \odot \mathbf{X}^*\|_F^2 + \|(\mathbf{1} - \mathbf{T}_2) \odot \mathbf{N}^*\|_F^2$ (first part of the cost function) among these 4-tuples is denoted by ε . Mathematically, ε is defined as:

$$\begin{aligned} \varepsilon \triangleq \min_i & \|(\mathbf{1} - \mathbf{T}_1^i) \odot \mathbf{X}^{*i}\|_F^2 + \|(\mathbf{1} - \mathbf{T}_2^i) \odot \mathbf{N}^{*i}\|_F^2. \\ \text{s.t.} & \|(\mathbf{1} - \mathbf{T}_1^i) \odot \mathbf{X}^{*i}\|_F^2 + \|(\mathbf{1} - \mathbf{T}_2^i) \odot \mathbf{N}^{*i}\|_F^2 \neq 0. \end{aligned} \quad (10)$$

Theorem 1. *Let the unique sparsest element of \mathbb{W} (solution of (2)) be $(\tilde{\mathbf{X}}, \tilde{\mathbf{N}})$ with respective supports $(\tilde{\mathbf{T}}_1, \tilde{\mathbf{T}}_2)$; moreover, let the sparsity numbers of $(\tilde{\mathbf{X}}, \tilde{\mathbf{N}})$ be $(\tilde{k}_1, \tilde{k}_2)$, then for $\lambda < \varepsilon / (\tilde{k}_1 + \tilde{k}_2)$, the minimizer of $f_\lambda(\mathbf{X}, \mathbf{N}, \mathbf{T}_1, \mathbf{T}_2)$ over \mathbb{W} is $(\tilde{\mathbf{X}}, \tilde{\mathbf{N}}, \tilde{\mathbf{T}}_1, \tilde{\mathbf{T}}_2)$.*

Proof: See Appendix B. ■

Now we discuss the uniqueness of the sparsest member of \mathbb{W} in Theorem 2.

Theorem 2. *The sparsest member of \mathbb{W} with sparsity numbers $(\tilde{k}_1, \tilde{k}_2)$ is unique if the following sufficient conditions are satisfied:*

$$\begin{cases} \mathbf{B}^T \otimes \mathbf{A} \text{ is orthonormal} \\ \tilde{k}_1 + \tilde{k}_2 < \frac{1}{2}(1 + \|\text{vec}(\mathbf{B}^T \otimes \mathbf{A})\|_\infty^{-1}) \end{cases} ; \quad (11)$$

where $(\cdot)^T$ and \otimes denote the transpose of a matrix and the Kronecker product of two matrices, respectively; the linear transformation $\mathcal{D}^{-1}(\mathbf{X}) = \mathbf{A} \mathbf{X} \mathbf{B}$; and $\|\text{vec}(\cdot)\|_\infty$ represents the L_∞ norm of the vectorization of the input, i.e., the entry with maximum absolute value.

Proof: See Appendix C. ■

When \mathcal{D}^{-1} is 2-dimensional inverse DCT (for images), we can easily conclude from Theorem 2 that $\tilde{k}_1 + \tilde{k}_2 < \frac{1}{2}(1 + \|\text{vec}(\mathbf{D} \otimes \mathbf{D})\|_\infty^{-1})$ guarantees the uniqueness of the sparsest member of \mathbb{W} , where \mathbf{D} is the DCT-matrix. In the case of square matrices, $\mathbf{D} \in \mathbb{R}^{m \times m}$, we have:

$$\begin{aligned} \|\text{vec}(\mathbf{D} \otimes \mathbf{D})\|_\infty &= (\|\text{vec}(\mathbf{D})\|_\infty)^2 = \\ &\begin{cases} \frac{2}{m} * \cos^2(\frac{\pi}{2m}) & m \text{ is power of } 2 \\ \frac{2}{m} & \text{o.w} \end{cases} ; \end{aligned} \quad (12)$$

Simulation results show that for much higher sparsity numbers, i.e., denser matrices, our algorithm still works.

C. Modifications

In this subsection, we proceed to introduce some modifications to our algorithm. The modified algorithm can be found in Algorithm 2. Note that the lines of the algorithm marked with (*) are only for image denoising and should be omitted in other applications. It is seen through simulation results that these modifications make the algorithm faster and improve the reconstruction quality.

In this algorithm, the inner loop and outer loop are merged. Furthermore, in the first algorithm, the signal and noise are first thresholded and then they are projected onto the set \mathbb{W} ; however, in the modified version, the signal is first thresholded and an approximation of the sparse noise is derived according to (1), then this approximated noise is thresholded and a better estimation of the signal is found by (1). It should also be noted that two different threshold levels, **th1** and **th2**, are

Algorithm 2 Modified IDT

```

1: Input:
2:   Observed matrix:  $\mathbf{Y} \in \mathbb{R}^{m \times n}$ 
3:   Four constants:  $\alpha_1, \beta_1, \alpha_2, \beta_2$ 
4:   Standard deviation of the gaussian filter:  $\sigma$  (*)
5:   Maximum number of iterations:  $K$ 
6:   Stopping threshold:  $\delta$ 
7: Output:
8:   Recovered estimate of the signal:  $\hat{\mathbf{X}} \in \mathbb{R}^{m \times n}$ 
9:   Recovered estimate of the noise:  $\hat{\mathbf{N}} \in \mathbb{R}^{m \times n}$ 
10: procedure
11:    $\mathbf{X}^0 \leftarrow \mathcal{D}(\mathbf{Y}), \quad \mathbf{N}^0 \leftarrow 0, \quad k \leftarrow 0$ 
12:   while  $e > \delta$  &  $k \leq K$  do
13:      $\mathbf{X}^k \leftarrow \text{threshold}(|\mathbf{X}_{i,j}^k|_{i=1,j=1}^{m,n}, \beta_1 e^{-\alpha_1 k})$ 
14:      $\mathbf{X}^k \leftarrow \text{clip}(\mathcal{D}^{-1}(\mathbf{X}^k))$  (*)
15:      $\mathbf{X}^k \leftarrow \text{gaussian-filter}(\mathbf{X}^k, \sigma)$  (*)
16:      $\mathbf{N}^{k+1} \leftarrow \mathbf{Y} - \mathbf{X}^k$ 
17:      $\mathbf{N}^{k+1} \leftarrow \text{threshold}(|\mathbf{N}_{i,j}^{k+1}|_{i=1,j=1}^{m,n}, \beta_2 e^{-\alpha_2 k})$ 
18:      $\mathbf{X}^{k+1} \leftarrow \mathcal{D}(\mathbf{Y} - \mathbf{N}^{k+1})$ 
19:      $e \leftarrow \|\mathbf{N}^{k+1} - \mathbf{N}^k\|_F$ 
20:      $k \leftarrow k + 1$ 
21:   end while
22:   return  $\hat{\mathbf{X}} \leftarrow \mathbf{X}^k, \hat{\mathbf{N}} \leftarrow \mathbf{N}^k$ 
23: end procedure

```

considered for signal and noise. **th1** and **th2** can be any decreasing sequences, but as is common in other papers [25]–[27], we adopted the exponential scheme to decrease them in each iteration.

In the image processing context, the reconstruction is not perfect since images do not become purely sparse by DCT or other transforms used to make the images sparse such as Wavelet and Contourlet. Nevertheless, two pieces of side information are available, i.e., the signal values are in the interval $[0, 255]$ for 8-bit images and the signal contains a large low frequency component. We can take advantage of the first one and clip the estimated signal in each iteration. Since the thresholding function is non-linear and changes the range of the signal and noise, this modification will result in a better reconstruction. In other words, we are considering the matrices with entries in $[0, 255]$ and project our approximated signal onto this convex set in each iteration. Moreover, we can apply a low-pass filter, to the signal so as to emphasize the low-pass component of the image and attenuate the high frequency components of the noise. Various filters were tested such as gaussian filter, median filter, adaptive median filter, non-local means [28] and guided image filter [29]. Gaussian filter was selected due to its best performance in our algorithm. It is worth noting that the filtering step can also be used in audio reconstruction.

III. SIMULATION RESULTS

We evaluate the effectiveness of our algorithm for different scenarios, i.e., images, audio and artificial sparse signals. Simulations are conducted in MATLAB 2018a on a PC equipped with an Intel Core i-7 3.60GHZ CPU and 64-GB RAM.

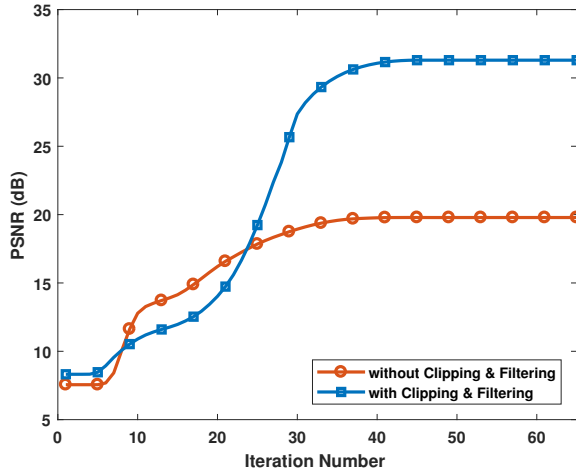


Fig. 1. Effect of clipping and filtering for the case of 50% salt-and-pepper noise for the Cropped Lena image.

A. Parameter Setting

We have 6 parameters in our algorithm: parameters of thresholding: $\alpha_1, \beta_1, \alpha_2, \beta_2$, standard deviation of the Gaussian filter: σ and number of iterations: K . The thresholding parameters depend on the absolute values of the signal and noise in their respective sparse domain. As is common in impulsive noise removal literature, in order to obtain a coarse estimation of the signal and noise, the adaptive median filters AMF [16] and ACWMF [21] are applied to the observed noisy signal in the case of SPN and RVIN, respectively. The absolute value of the samples of the estimated signal and noise (in their sparse domain) with maximum absolute values are good choices for β_1 and β_2 . Moreover, If we sort the samples of the estimated signal and noise based on their absolute values, the averages of the difference between two consecutive samples are good choices for α_1 and α_2 . We have come to this setting based on our experience: Our algorithm finds the larger components of the sparse signal in the first few iterations and by decreasing the threshold level, the lower components are found. Therefore, the proposed process of defining the parameters of thresholding seem reasonable and it works well in practice. As the standard deviation of the Gaussian filter increases, the lower frequencies of the image are affected (the smoothing effect is higher). Hence, when the impulsive noise density is low, we use $\sigma = 0.4$ and in the case of higher noise densities, we use $\sigma = 0.55$. Finally, if the thresholding parameters are defined in a good manner, after at most $K = 60$ iterations our algorithm converges. As K signifies the run-time of the algorithm, we would like to minimize this parameter.

B. Artificial Sparse Signal and Noise

In this subsection, we generate a 500×500 2-D signal which is sparse in DCT domain and a 500×500 sparse noise. The sparse elements of the signal and noise are independently sampled from a normal distribution with variance 128. We evaluate the performance of our algorithm in terms of Success Rate (SR) and SNR. A reconstruction is considered as a

TABLE I
RECONSTRUCTION SNR (dB) AND SR (IN THE BRACKET) FOR DIFFERENT SIGNAL (ρ_x) AND NOISE SPARSITY RATIOS (ρ_n)

$\rho_x \backslash \rho_n$	10%	20%	30%
10%	316.5 (100%)	313.5 (100%)	311.6 (100%)
20%	315.9 (100%)	312.6 (100%)	310.4 (100%)
30%	314.9 (100%)	311.4 (100%)	224.082 (73%)

success if the output SNR is greater than 60 dB. The results are presented in Table I for different signal and noise sparsity ratios $\rho = \text{Sparsity Number}/500^2$. As can be seen in this table, when the sparsity ratio of both signal and noise are 30%, the success rate falls despite the fact that the average SNR is still high. In order to explain this phenomenon, let the sparsity ratio of one of the signals be 30%. Since the location and the value of these entries are unknown, there are about 60% unknown variables and at least 60% equations are needed to find the unknown variables. If the location of the non-zero entries of the other signal was known, its sparsity ratio could have been 40%. However, in our case where no side information about the sparsity of the signals is provided, the sparsity ratio should be less than 40%. Table I shows that when the signal and noise are purely sparse, our algorithm can fully reconstruct the signal.

C. Impulsive Noise Removal from Images

The most common type of impulsive noise in image processing is SPN. The noisy pixels in the image corrupted by this type of noise take the maximum or minimum values of the image, i.e., zero or 255 in 8-bit-per-pixel images. Since images are almost sparse in the DCT domain, as an example of sparse noise removal from 2-D signals, we add SPN to some images and employ Algorithm 2 for denoising. One should note that if we use wavelets or contourlets instead of DCT, the Peak Signal to Noise Ratio (PSNR) may be at most 0.2 dB better but the computation time is much longer. Therefore, the results of the DCT transformation are only reported. Furthermore, unknown missing samples are a special case of the SPN (the probability of salt is zero) and the quality is about the same as that of SPN. The output PSNR for 256×256 cropped Lena image corrupted by 50% SPN after each iteration of algorithm 2 with or without clipping plus gaussian filtering is depicted in Fig. 1. As can be seen, the clipping and gaussian filtering technique result in a better reconstruction. We compare our results with AMF [16] with maximum window size of 19, TPF [18] and WESNR [22]. The restoration results in terms of PSNR and Structural Similarity Metric (SSIM) [30] for the 512×512 images distorted with various densities of SPN are reported in Table II. This table shows that our algorithm outperforms the other methods in terms of SSIM and subjective evaluation for all images and noise densities. As the PSNR metric is concerned, the IDT algorithm is better than all the other methods except the WESNR, which is at most 1.5 dB better in the case of *Peppers*, *F-16* and *Boats* images for 40% or 50% noise densities. Figure 2 exhibits the restored images of various methods for the *Baboon* image corrupted by 50%

TABLE II
PSNR AND SSIM FOR DIFFERENT SALT-AND-PEPPER NOISE DENSITIES

Noise Densities		PSNR					SSIM				
		10%	20%	30%	40%	50%	10%	20%	30%	40%	50%
Lena	AMF	38.27	35.9	33.56	31.87	30.39	0.9628	0.9545	0.9389	0.9174	0.8908
	TPFF	35.78	35.06	32.79	30.98	29.71	NOT AVAILABLE				
	WESNR	35.91	35.56	35.11	34.52	33.61	0.9151	0.9134	0.9099	0.9045	0.8963
	IDT	43.35	39.90	37.56	35.45	33.54	0.9901	0.9792	0.9676	0.9527	0.9341
Peppers	AMF	36.06	33.98	32.17	30.67	29.23	0.9482	0.9410	0.9257	0.9021	0.8733
	TPFF	35.80	33.45	31.27	29.21	28.00	NOT AVAILABLE				
	WESNR	35.01	34.59	34.08	33.34	32.49	0.8842	0.8834	0.8818	0.8785	0.8727
	IDT	38.64	35.76	33.65	31.85	30.91	0.9811	0.9634	0.9402	0.9152	0.8891
F-16	AMF	35.87	32.97	31.05	29.43	27.77	0.9780	0.9699	0.9560	0.9377	0.9118
	TPFF	35.78	32.83	30.72	29.18	28.01	NOT AVAILABLE				
	WESNR	35.27	34.64	33.96	32.80	31.85	0.9382	0.9361	0.9322	0.9264	0.9187
	IDT	41.00	37.64	34.65	31.71	30.56	0.9814	0.9651	0.9539	0.9413	0.9284
Baboon	AMF	26.95	25.73	24.53	23.29	22.14	0.8922	0.8717	0.8351	0.7866	0.7264
	TPFF	30.96	27.90	26.34	25.15	23.87	NOT AVAILABLE				
	WESNR	26.44	26.17	25.70	24.93	24.11	0.7982	0.7938	0.7784	0.7529	0.7170
	IDT	32.41	29.24	27.17	25.60	24.38	0.9751	0.9449	0.9088	0.8654	0.8116
Boat	AMF	33.94	32.05	30.25	28.74	27.16	0.9345	0.9215	0.8986	0.8679	0.8274
	TPFF	NOT AVAILABLE									
	WESNR	32.78	32.40	31.84	31.13	30.08	0.8659	0.8635	0.8567	0.8478	0.8317
	IDT	37.91	34.91	32.68	30.77	29.15	0.9791	0.9579	0.9340	0.9082	0.8744

SPN. This figure shows that the TPFF and AMF algorithms are not capable of completely removing the noise and the WESNR algorithm smoothes the image but our proposed method preserves the details of the image and remove the noise completely.

As another example of sparse noise, we consider RVIN. In this case, each noisy pixel randomly takes a value in the interval $[0, 255]$ with uniform distribution. We compare our algorithm with the methods called ACWMF [21], WESNR [22], SAFE [20] and ALOHA [23]. The results can be found in Table III. Our algorithm is better than or equal to the other methods in terms of the SSIM when the noise density is less than 30%, but the SAFE algorithm is slightly better for higher noise densities. Moreover, the IDT algorithm outperforms all the other methods for the *F-16* and *Baboon* images and all RVIN densities in terms of PSNR. For other images, from PSNR point of view, our algorithm is more or less the same as the ALOHA algorithm when the noise density is less than 30%, and for higher noise densities, the IDT algorithm is more or less the same as the SAFE algorithm. The ALOHA and the SAFE algorithms do not work well for SPN removal, and it is demonstrated in the next subsection that the run-time of our algorithm is much less than these two methods. The restored images for the *peppers* image corrupted by 40% RVIN are depicted in Figure 3. This figure shows that the ACWMF and the WESNR algorithms are not capable of removing all the impulsive noise. The ALOHA algorithm adds some artifacts to the image and the SAFE and the proposed algorithm have the same subjective quality. Our algorithm also performs well when the image is corrupted by mixed RVIN and SPN. The results for the *F-16* image corrupted by 15% SPN and 25% RVIN can be found in Figure 4. The proposed algorithm can easily be applied to colored images by denoising each channel separately. As an example, the colored *Lena* image is corrupted by 30% RVIN and the reconstructed image is depicted in 5.

D. Audio Reconstruction

Clicks and pops are localized bursts of impulsive noise in audio signals and they are commonly caused by particles or scratches on the surface of a phonograph record or CD. In the recent publications in impulsive noise removal from audio signals [31], [32], it is assumed that the noisy samples are detected beforehand, and thus it is not fair to compare our results with theirs. As an example of impulsive noise removal from 1-D signals, we use IDT algorithm to remove clicks from a 5 second of the country music '*you are my sunshine*' [33]. The noisy and reconstructed audio signals are presented in Figure 6. The SNR and Perceptual Evaluation of Audio Quality (PEAQ) are given in the same figure. For the quality of the restored audio signal, please check 'acri.ee.sharif.ir'.

E. Complexity

We evaluate the complexity of our method in terms of the run-time in this subsection. The simulation is conducted for the *Lena* image corrupted with 30% densities of impulsive noise. The results are shown in Table IV. This table shows that our method is very efficient and fast. On the other hand, the SAFE and ALOHA algorithms are extremely inefficient while the WESNR method is about 20 times slower than IDT. In each iteration of the proposed method, there are one 2D-DCT, one 2D-IDCT, two thresholding, one clipping and one gaussian filtering. The dominant terms in computational complexity are 2D-DCT and 2D-IDCT, and hence the overall complexity of our algorithm is $\mathcal{O}(n^2) \log n$ [34].

IV. CONCLUSION

In this paper, we proposed a new method for separating two signal that are sparse in two different domains. Among the applications of this problem are removal of impulsive

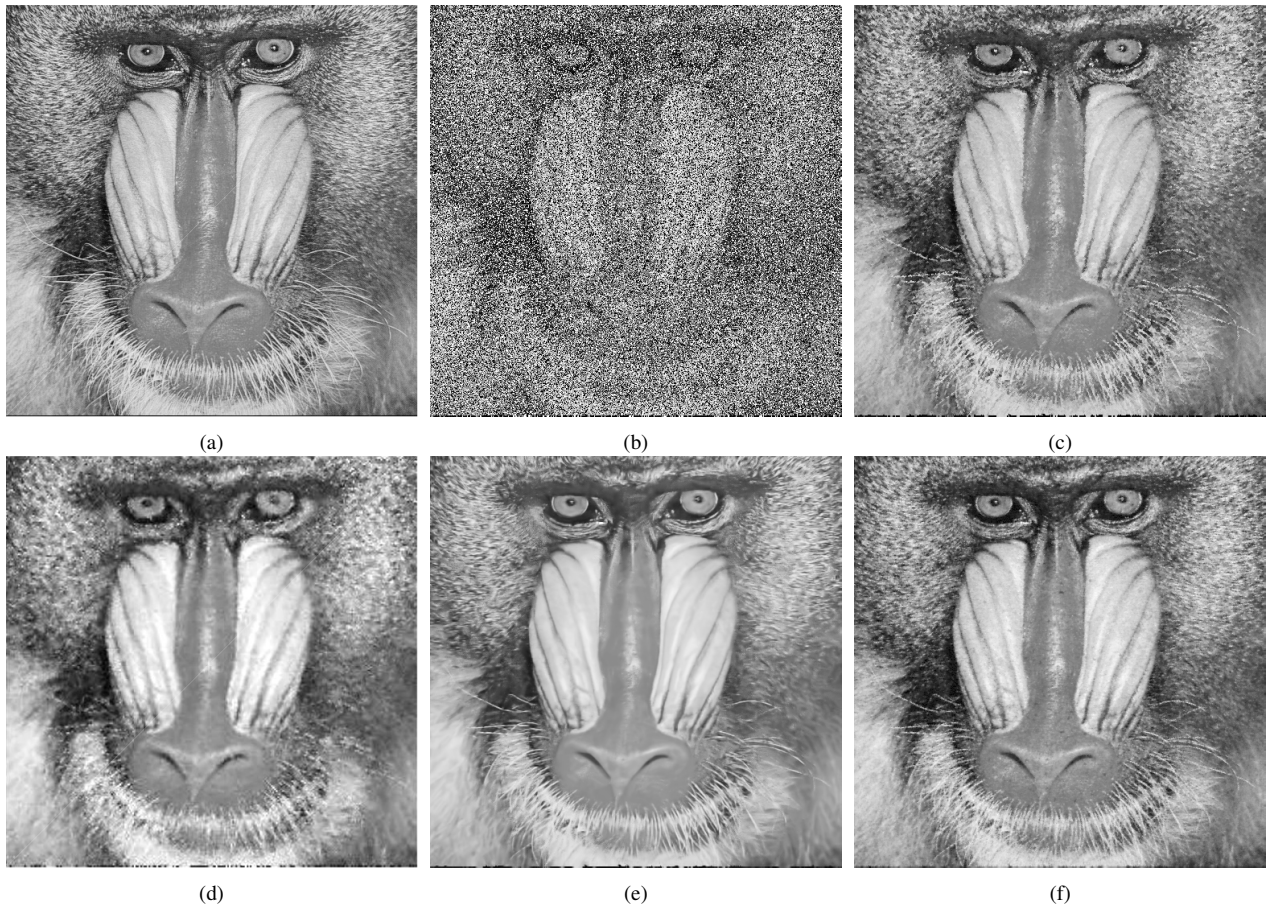


Fig. 2. Reconstructed images using different methods for the *Baboon* image corrupted by 50% SPN. (a) Original image (b) Noisy image, (c) AMF 19×19 , (d) TPF, (e) WESNR, (f) IDT.

TABLE III
PSNR AND SSIM FOR DIFFERENT RANDOM-VALUED IMPULSIVE NOISE DENSITIES (ND)

Noise Densities		PSNR						SSIM					
		5%	10%	20%	30%	40%	50%	5%	10%	20%	30%	40%	50%
Lena	ACWMF	38.53	35.32	31.61	28.76	26.15	23.52	0.9669	0.9325	0.8562	0.7592	0.6459	0.5133
	WESNR	36.83	36.30	35.10	33.00	30.91	28.18	0.9271	0.9245	0.9165	0.8972	0.8619	0.7880
	SAFE	34.97	35.92	34.79	33.33	31.97	30.43	0.9587	0.9635	0.9551	0.9407	0.9208	0.8930
	ALOHA	40.79	38.81	35.32	32.66	30.62	26.69	0.9821	0.9695	0.9403	0.9023	0.8752	0.7729
	IDT	40.10	37.75	34.88	32.97	31.34	29.73	0.9839	0.9732	0.9516	0.9293	0.9023	0.8712
Peppers	ACWMF	36.73	34.30	30.56	27.85	25.06	22.23	0.9659	0.9311	0.8494	0.7469	0.6201	0.4819
	WESNR	35.31	34.68	33.61	31.83	29.13	26.01	0.8955	0.8949	0.8888	0.8752	0.8342	0.7398
	SAFE	30.56	30.80	30.40	29.82	28.97	28.40	0.9492	0.9537	0.9423	0.9151	0.8742	0.8812
	ALOHA	37.55	35.91	33.00	31.16	28.50	25.02	0.9585	0.9310	0.8759	0.8337	0.7767	0.6824
	IDT	37.40	35.20	32.10	31.00	29.53	27.92	0.9770	0.9653	0.9303	0.9151	0.8850	0.8461
F-16	ACWMF	36.78	33.62	29.95	27.28	24.57	21.72	0.9700	0.9351	0.8561	0.7576	0.6220	0.4784
	WESNR	35.75	34.80	32.85	30.72	28.37	25.44	0.9453	0.9420	0.9321	0.9115	0.8601	0.7511
	SAFE	28.29	28.81	28.64	28.02	27.31	26.47	0.9498	0.9525	0.9447	0.9188	0.8804	0.8898
	ALOHA	36.17	34.93	32.26	28.33	27.76	24.68	0.9410	0.9255	0.9072	0.8788	0.8633	0.7503
	IDT	38.28	35.77	32.75	30.65	28.81	27.05	0.9853	0.9771	0.9595	0.9382	0.9113	0.8741
Baboon	ACWMF	27.63	26.31	24.37	22.64	21.28	19.83	0.9311	0.8955	0.8214	0.7299	0.6329	0.5171
	WESNR	26.90	26.12	24.86	23.76	22.62	21.42	0.8420	0.8251	0.7852	0.7402	0.6761	0.5931
	SAFE	24.02	24.57	24.26	23.35	22.24	21.19	0.8217	0.8558	0.8382	0.7827	0.7126	0.6305
	ALOHA	29.37	28.59	25.56	22.66	22.33	20.56	0.7721	0.7716	0.7015	0.6495	0.6433	0.5792
	IDT	30.86	28.26	25.50	23.83	22.50	21.43	0.9446	0.9061	0.8340	0.7604	0.6800	0.6069
Boat	ACWMF	34.65	32.29	29.15	26.86	24.64	22.31	0.9633	0.9274	0.8476	0.7545	0.6451	0.5193
	WESNR	33.13	32.55	31.24	29.58	27.85	25.72	0.8892	0.8835	0.8675	0.8387	0.7945	0.7161
	SAFE	30.19	31.33	30.65	29.26	28.04	26.62	0.9171	0.9377	0.9187	0.8922	0.8560	0.8051
	ALOHA	35.88	34.53	31.11	29.47	26.99	24.29	0.9574	0.9536	0.8869	0.8571	0.7594	0.6818
	IDT	35.02	33.01	30.58	28.91	27.65	25.88	0.9688	0.9505	0.9148	0.8781	0.8371	0.7876

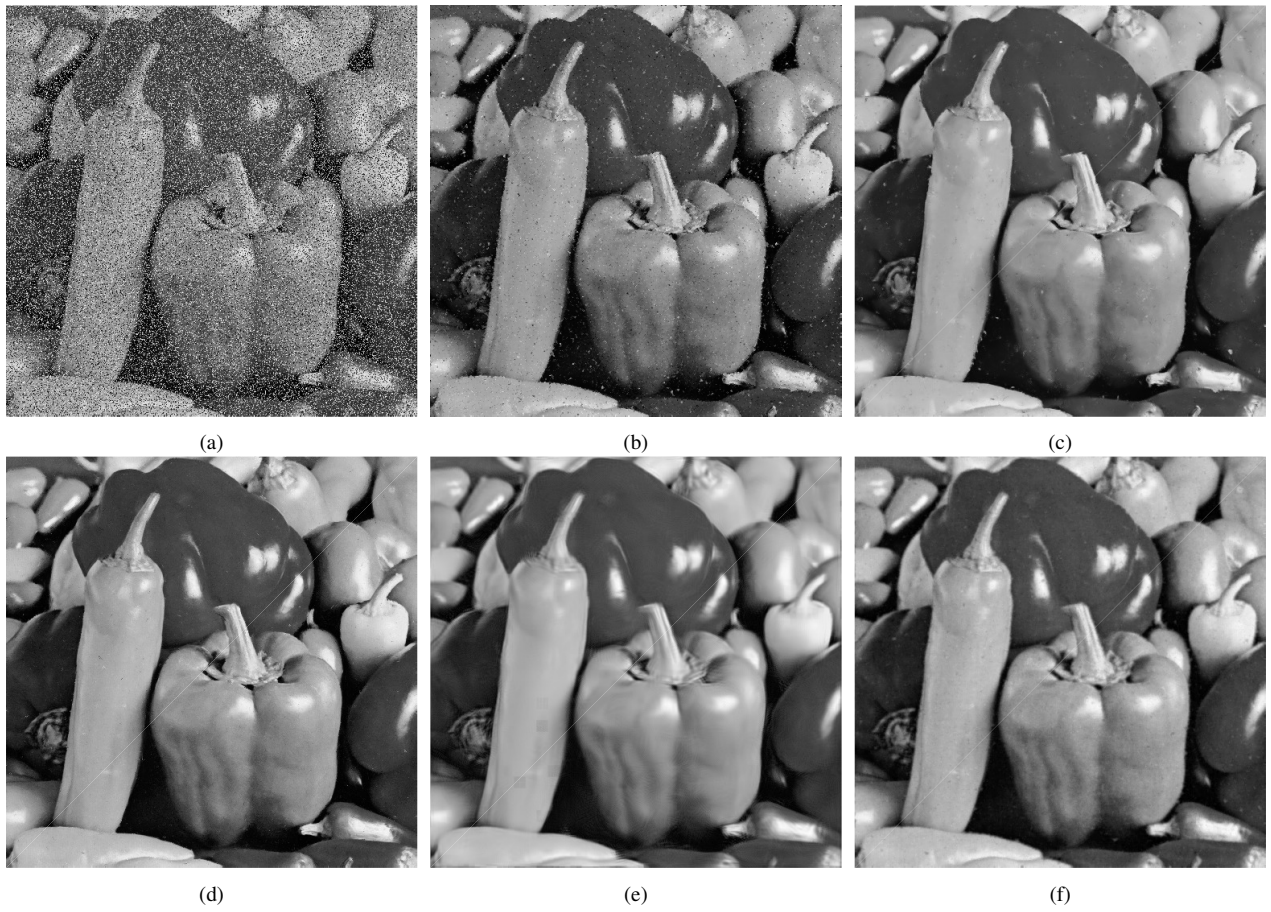


Fig. 3. Reconstructed images using different methods for the *Peppers* image corrupted by 40% random-valued impulsive noise. (a) Noisy image, (b) ACWMF, (c) WESNR, (d) SAFE, (e) ALOHA, (f) IDT.

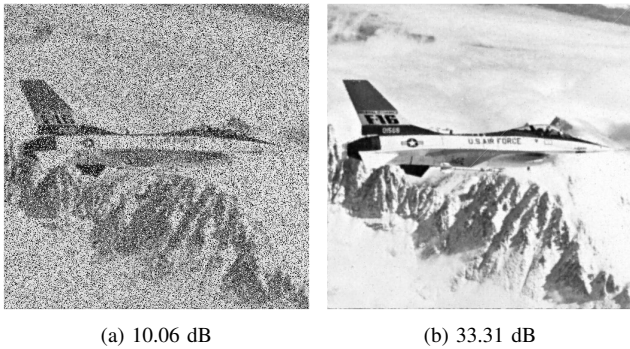


Fig. 4. Restored images for the *F-16* image corrupted by 15% RVIN and 25% SPN. (a) Noisy image, (b) Restored image.

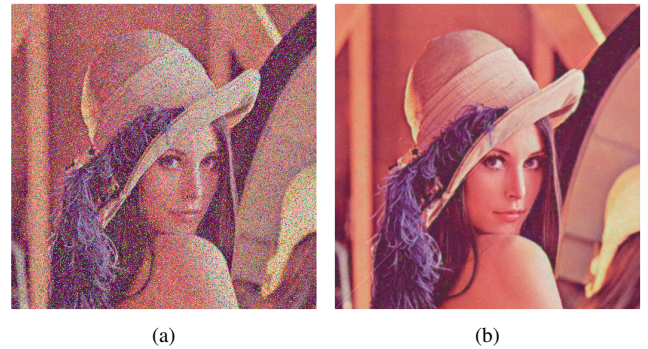


Fig. 5. Restored images for the colored *Lena* image corrupted by 30% RVIN. (a) Noisy image, (b) Restored image.

TABLE IV
RUN-TIME OF DIFFERENT METHODS IN SECONDS

AMF	ACWMF	TPFF	WESNR	SAFE (on GPU)	ALOHA on GPU	IDT
1.13	1.94	1.75	34.32	763.48 (21.07)	1368.2	1.71

noise from images and clicks from audio signals. Two iterative algorithms were developed to minimize a proposed cost function. We evaluated different aspects of our method through numerical experiments with comparison to other well-known

methods. We observed that our algorithm is fast and suitable for real-time applications and it outperforms the other methods in terms of the reconstruction quality and/or complexity. For images, the proposed algorithm works for any type of impulsive noise as opposed to other well-known methods that are suitable for either SPN or RVIN. For Future work, we can consider sparse noise in videos and block sparse noises such as block losses in the JPEG and MPEG images. Moreover, we wish to continue on this topic using machine learning techniques. We are currently working on soft thresholding that may improve the performance of recovery.

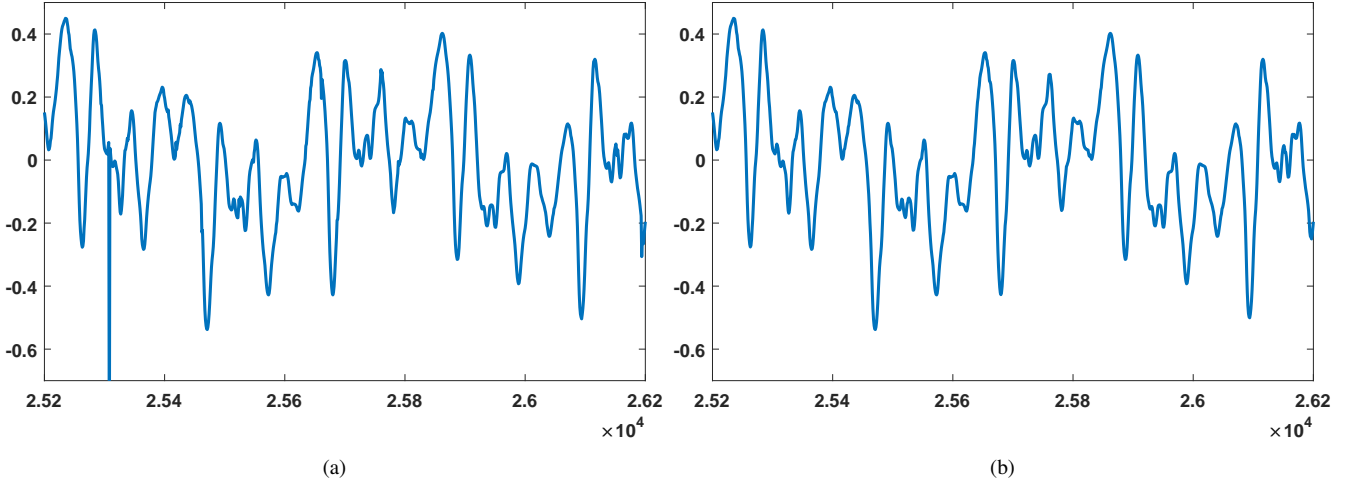


Fig. 6. Recovery of audio degraded with clicks. (a) Degraded audio (SNR = 26.27 dB, PEAQ = 2.45), (b) Restored audio (SNR = 35.55, PEAQ = 1.11).

APPENDIX A PROOF OF LEMMA 1

In order to compute this projection, we denote the concatenation of two matrices \mathbf{U}, \mathbf{V} by $[\mathbf{U}, \mathbf{V}]$, and show the Frobenius inner product of two matrices, i.e., trace of their product, by $\langle \mathbf{U}, \mathbf{V} \rangle$.

Lemma 2. *If \mathcal{D} is an orthogonal transformation, then $\langle [\mathcal{D}(\mathbf{U}), \mathbf{U}], [\mathcal{D}(-\mathbf{V}), \mathbf{V}] \rangle = 0$.*

Proof:

$$\begin{aligned} \langle [\mathcal{D}(\mathbf{U}), \mathbf{U}], [\mathcal{D}(-\mathbf{V}), \mathbf{V}] \rangle &= \langle \mathcal{D}(\mathbf{U}), \mathcal{D}(-\mathbf{V}) \rangle + \langle \mathbf{U}, \mathbf{V} \rangle \\ &= \langle \mathbf{U}, -\mathbf{V} \rangle + \langle \mathbf{U}, \mathbf{V} \rangle = 0. \end{aligned} \quad (13)$$

In order for $(\hat{\mathbf{X}}, \hat{\mathbf{N}})$ to be the projection of (\mathbf{X}, \mathbf{N}) onto the set W , the error $(\mathbf{X}, \mathbf{N}) - (\hat{\mathbf{X}}, \hat{\mathbf{N}})$ has to be orthogonal to the set, i.e., it has to be orthogonal to the difference of any two members of W . The difference of any two members of W is $(\mathcal{D}(\mathbf{Y} - \mathbf{U}_1), \mathbf{U}_1) - (\mathcal{D}(\mathbf{Y} - \mathbf{U}_2), \mathbf{U}_2) = (\mathcal{D}(\mathbf{U}_2 - \mathbf{U}_1), \mathbf{U}_1 - \mathbf{U}_2)$, which is of the form $(\mathcal{D}(-\mathbf{V}), \mathbf{V})$. By employing Lemma 2, the error $(\mathbf{X}, \mathbf{N}) - (\hat{\mathbf{X}}, \hat{\mathbf{N}})$ has to be of the form $(\mathcal{D}(\mathbf{U}), \mathbf{U})$, where \mathbf{U} is an auxiliary variable, so that the orthogonality is assured. Specifically:

$$\begin{cases} (\mathbf{X}, \mathbf{N}) - (\hat{\mathbf{X}}, \hat{\mathbf{N}}) = (\mathcal{D}(\mathbf{U}), \mathbf{U}) \\ \mathcal{D}^{-1}(\hat{\mathbf{X}}) + \hat{\mathbf{N}} = \mathbf{Y} \end{cases} \quad (14)$$

The first equality holds as a result of Lemma 2. The second equality also holds since $(\hat{\mathbf{X}}, \hat{\mathbf{N}}) \in W$. One can easily omit the auxiliary variable \mathbf{U} and obtain the desired result.

APPENDIX B PROOF OF THEOREM 1

Before we proceed with the proof, let $(\mathbf{X}^*, \mathbf{N}^*)$, with respective sparsity numbers of (k_1, k_2) , be the minimizers of f_λ for a given pair of $(\mathbf{T}_1, \mathbf{T}_2)$. We will show that the cost function (4) has greater values for binary matrices $(\mathbf{T}_1, \mathbf{T}_2)$ other than $(\hat{\mathbf{T}}_1, \hat{\mathbf{T}}_2)$. To this aim, we consider two cases:

Case 1:

$$\|(\mathbf{1} - \mathbf{T}_1) \odot \mathbf{X}^*\|_F = 0 \text{ and } \|(\mathbf{1} - \mathbf{T}_2) \odot \mathbf{N}^*\|_F = 0 \quad (15)$$

Case 2:

$$\|(\mathbf{1} - \mathbf{T}_1) \odot \mathbf{X}^*\|_F \neq 0 \text{ or } \|(\mathbf{1} - \mathbf{T}_2) \odot \mathbf{N}^*\|_F \neq 0 \quad (16)$$

In the first case, we will show that $\|\text{vec}(\mathbf{T}_1)\|_1 + \|\text{vec}(\mathbf{T}_2)\|_1 \geq \tilde{k}_1 + \tilde{k}_2$. Assume the opposite, that is:

$$\|\text{vec}(\mathbf{T}_1)\|_1 + \|\text{vec}(\mathbf{T}_2)\|_1 \leq \tilde{k}_1 + \tilde{k}_2 - 1, \quad (17)$$

then $(\mathbf{1} - \mathbf{T}_1)$ and $(\mathbf{1} - \mathbf{T}_2)$ has at most $\tilde{k}_1 + \tilde{k}_2 - 1$ zero entries in total. Therefore, in order for (15) to be true, \mathbf{X}^* and \mathbf{N}^* can have at most $\tilde{k}_1 + \tilde{k}_2 - 1$ non-zero entries in the corresponding zero elements of $(\mathbf{1} - \mathbf{T}_1)$ and $(\mathbf{1} - \mathbf{T}_2)$, respectively, in other words:

$$\begin{aligned} \|\text{vec}(\mathbf{X}^*)\|_0 + \|\text{vec}(\mathbf{N}^*)\|_0 &\leq \tilde{k}_1 + \tilde{k}_2 - 1 \Rightarrow \\ k_1 + k_2 &\leq \tilde{k}_1 + \tilde{k}_2 - 1. \end{aligned} \quad (18)$$

Based on the assumption of the uniqueness of the sparsest solution, the sum of the sparsity numbers of every members of W , except the sparsest one, is more than $\tilde{k}_1 + \tilde{k}_2$; since $(\mathbf{X}^*, \mathbf{N}^*) \in W$, a contradiction is found. Consequently $\|\text{vec}(\mathbf{T}_1)\|_1 + \|\text{vec}(\mathbf{T}_2)\|_1 \geq \tilde{k}_1 + \tilde{k}_2$, and the equality only holds for the sparsest member.

In the second case, since (16) holds according to the definition ε in (10), we have:

$$\|(\mathbf{1} - \mathbf{T}_1^i) \odot \mathbf{X}^{*i}\|_F^2 + \|(\mathbf{1} - \mathbf{T}_2^i) \odot \mathbf{N}^{*i}\|_F^2 \geq \varepsilon > \lambda(\tilde{k}_1 + \tilde{k}_2). \quad (19)$$

One can easily see that in both cases, for all the members of W , except for the sparsest one, $f_\lambda(\mathbf{X}, \mathbf{N}, \mathbf{T}_1, \mathbf{T}_2) > \lambda(\tilde{k}_1 + \tilde{k}_2) = f_\lambda(\hat{\mathbf{X}}, \hat{\mathbf{N}}, \hat{\mathbf{T}}_1, \hat{\mathbf{T}}_2)$. Hence the minimizer of f_λ is indeed the sparsest member of W .

APPENDIX C PROOF OF THEOREM 2

We use the following lemma in order to prove the theorem by contradiction.

Lemma 3. Let Φ_1 and Φ_2 be orthonormal bases for \mathbb{R}^N and let

$$M(\Phi_1, \Phi_2) = \sup\{|\langle \Phi_1, \Phi_2 \rangle| \mid \Phi_1 \in \Phi_1, \Phi_2 \in \Phi_2\}.$$

Let Γ_1 be the set of indices of non-zero coefficients for \mathbf{x} in basis 1, and Γ_2 be the set of indices of non-zero coefficients for \mathbf{x} in basis 2. Then

$$|\Gamma_1| + |\Gamma_2| \geq (1 + M^{-1}). \quad (20)$$

Proof: See Theorem 7.3 in [24]. ■

Assume otherwise, that is, assume that there exists two members in W with sparsity numbers $(\tilde{k}_1, \tilde{k}_2)$ and they are denoted by $(\mathbf{X}_1, \mathbf{N}_1)$ and $(\mathbf{X}_2, \mathbf{N}_2)$.

$$\begin{aligned} \mathcal{D}^{-1}(\mathbf{X}_1) + \mathbf{N}_1 &= \mathcal{D}^{-1}(\mathbf{X}_2) + \mathbf{N}_2 = \mathbf{Y} \Rightarrow \\ \mathcal{D}^{-1}(\mathbf{X}_1 - \mathbf{X}_2) + (\mathbf{N}_1 - \mathbf{N}_2) &= \mathbf{0} \Rightarrow \\ \mathbf{A}(\mathbf{X}_1 - \mathbf{X}_2)\mathbf{B} + (\mathbf{N}_1 - \mathbf{N}_2) &= \mathbf{0}; \end{aligned} \quad (21)$$

by defining $\mathbf{X}' = \mathbf{X}_1 - \mathbf{X}_2$ and $\mathbf{N}' = \mathbf{N}_1 - \mathbf{N}_2$, with maximum sparsity numbers of $2\tilde{k}_1$ and $2\tilde{k}_2$, respectively, we will have:

$$\begin{aligned} \mathbf{A}\mathbf{X}'\mathbf{B} + \mathbf{N}' &= \mathbf{0} \Rightarrow \\ \text{vec}(\mathbf{A}\mathbf{X}'\mathbf{B}) + \text{vec}(\mathbf{N}') &= \mathbf{0} \Rightarrow \\ (\mathbf{B}^T \otimes \mathbf{A})\text{vec}(\mathbf{X}') + \text{vec}(\mathbf{N}') &= \mathbf{0}; \end{aligned} \quad (22)$$

if $\mathbf{x} = \text{vec}(\mathbf{X}')$, $\mathbf{n} = \text{vec}(\mathbf{N}')$ and $\mathbf{C} = \mathbf{B}^T \otimes \mathbf{A} \in \mathbb{R}^{mn \times mn}$, we can conclude that:

$$\mathbf{x} = -\mathbf{C}^{-1} \mathbf{n} = -\mathbf{C}^T \mathbf{n}; \quad (23)$$

in other words, $-\mathbf{n}$ is the representation of \mathbf{x} in the orthonormal basis \mathbf{C} . According to Lemma 3, if \mathbf{x} has N_I and N_C non-zero coefficients in orthonormal bases \mathbf{I} (Identity matrix) and \mathbf{C} , respectively, then $N_I + N_C \geq (1 + M(\mathbf{I}, \mathbf{C})^{-1})$. Therefore:

$$\begin{aligned} \|\mathbf{x}\|_0 + \|\mathbf{n}\|_0 &= 2\tilde{k}_1 + 2\tilde{k}_2 \geq \\ 1 + M(\mathbf{I}, \mathbf{C})^{-1} &= 1 + \|\text{vec}(\mathbf{B}^T \otimes \mathbf{A})\|_\infty^{-1}, \end{aligned} \quad (24)$$

which contradicts (11). Hence, $\mathbf{x} = \mathbf{0}$ and $\mathbf{n} = \mathbf{0}$. Since \mathbf{x} and \mathbf{n} are the vectorization of \mathbf{X}' and \mathbf{N}' , respectively, $\mathbf{X}' = \mathbf{X}_1 - \mathbf{X}_2 = \mathbf{0}$ and $\mathbf{N}' = \mathbf{N}_1 - \mathbf{N}_2 = \mathbf{0}$. The uniqueness of the sparsest member of W is then concluded.

REFERENCES

- [1] S. Zahedpour, S. Feizi, A. Amini, M. Ferdosizadeh, and F. Marvasti, "Impulsive noise cancellation based on soft decision and recursion," *IEEE Transactions on instrumentation and measurement*, vol. 58, no. 8, pp. 2780–2790, 2009.
- [2] H. Hosseini, F. Hesar, and F. Marvasti, "Real-time impulse noise suppression from images using an efficient weighted-average filtering," *IEEE Signal Processing Letters*, vol. 22, no. 8, pp. 1050–1054, 2015.
- [3] K. K. V. Toh and N. A. M. Isa, "Noise adaptive fuzzy switching median filter for salt-and-pepper noise reduction," *IEEE signal processing letters*, vol. 17, no. 3, pp. 281–284, 2010.
- [4] N. Kim, H.-G. Byun, Y.-H. You, and K. Kwon, "Blind signal processing for impulsive noise channels," *Journal of Communications and Networks*, vol. 14, no. 1, pp. 27–33, 2012.
- [5] J. Lyu, D. Bi, X. Li, and Y. Xie, "Robust compressive 2-d near-field millimeter-wave image reconstruction in impulsive noise," *IEEE Signal Processing Letters*, 2019.

- [6] L. Gao, X. Li, D. Bi, and Y. Xie, "A q -gaussian maximum correntropy adaptive filtering algorithm for robust sparse recovery in impulsive noise," *IEEE Signal Processing Letters*, vol. 25, no. 12, pp. 1770–1774, 2018.
- [7] A. Javaheri, H. Zayyani, M. A. Figueiredo, and F. Marvasti, "Robust sparse recovery in impulsive noise via continuous mixed norm," *IEEE Signal Processing Letters*, vol. 25, no. 8, pp. 1146–1150, 2018.
- [8] N. Zarmehi and F. Marvasti, "Sparse and low-rank recovery using adaptive thresholding," *Digital Signal Processing*, vol. 73, pp. 145–152, 2018.
- [9] S. Oymak, A. Jalali, M. Fazel, Y. C. Eldar, and B. Hassibi, "Simultaneously structured models with application to sparse and low-rank matrices," *IEEE Transactions on Information Theory*, vol. 61, no. 5, pp. 2886–2908, 2015.
- [10] A. Adler, V. Emiya, M. G. Jafari, M. Elad, R. Gribonval, and M. D. Plumbley, "Audio inpainting," *IEEE Transactions on Audio, Speech, and Language Processing*, vol. 20, no. 3, pp. 922–932, 2012.
- [11] A. Roy, J. Singha, S. S. Devi, and R. H. Laskar, "Impulse noise removal using svm classification based fuzzy filter from gray scale images," *Signal Processing*, vol. 128, pp. 262–273, 2016.
- [12] V. Gupta, V. Chaurasia, and M. Shandilya, "Random-valued impulse noise removal using adaptive dual threshold median filter," *Journal of Visual Communication and Image Representation*, vol. 26, pp. 296–304, 2015.
- [13] J. Wu and C. Tang, "Pde-based random-valued impulse noise removal based on new class of controlling functions," *IEEE transactions on image processing*, vol. 20, no. 9, pp. 2428–2438, 2011.
- [14] F. Ahmed and S. Das, "Removal of high-density salt-and-pepper noise in images with an iterative adaptive fuzzy filter using alpha-trimmed mean," *IEEE Trans. Fuzzy Systems*, vol. 22, no. 5, pp. 1352–1358, 2014.
- [15] H. Y. Khaw, F. C. Soon, J. H. Chuah, and C.-O. Chow, "High-density impulse noise detection and removal using deep convolutional neural network with particle swarm optimisation," *IET Image Processing*, 2018.
- [16] H. Hwang and R. A. Haddad, "Adaptive median filters: new algorithms and results," *IEEE Transactions on image processing*, vol. 4, no. 4, pp. 499–502, 1995.
- [17] F. R. Avila and L. W. Biscainho, "Bayesian restoration of audio signals degraded by impulsive noise modeled as individual pulses," *IEEE Transactions On Audio, Speech, And Language Processing*, vol. 20, no. 9, pp. 2470–2481, 2012.
- [18] H.-H. Chou, L.-Y. Hsu, and H.-T. Hu, "Turbulent-pso-based fuzzy image filter with no-reference measures for high-density impulse noise," *IEEE transactions on cybernetics*, vol. 43, no. 1, pp. 296–307, 2013.
- [19] J. Wu and C. Tang, "Random-valued impulse noise removal using fuzzy weighted non-local means," *Signal, Image and Video Processing*, vol. 8, no. 2, pp. 349–355, 2014.
- [20] Y. Chen, Y. Zhang, J. Yang, H. Shu, L. Luo, J.-L. Coatrieux, and Q. Feng, "Structure-adaptive fuzzy estimation for random-valued impulse noise suppression," *IEEE Transactions on Circuits and Systems for Video Technology*, 2018.
- [21] T. Chen and H. R. Wu, "Adaptive impulse detection using center-weighted median filters," *IEEE Signal Processing Letters*, vol. 8, no. 1, pp. 1–3, 2001.
- [22] J. Jiang, L. Zhang, and J. Yang, "Mixed noise removal by weighted encoding with sparse nonlocal regularization," *IEEE transactions on image processing*, vol. 23, no. 6, pp. 2651–2662, 2014.
- [23] K. H. Jin and J. C. Ye, "Sparse and low-rank decomposition of a hankel structured matrix for impulse noise removal," *IEEE Transactions on Image Processing*, vol. 27, no. 3, pp. 1448–1461, 2018.
- [24] D. L. Donoho and X. Huo, "Uncertainty principles and ideal atomic decomposition," *IEEE transactions on information theory*, vol. 47, no. 7, pp. 2845–2862, 2001.
- [25] M. Azghani, P. Kosmas, and F. Marvasti, "Microwave medical imaging based on sparsity and an iterative method with adaptive thresholding," *IEEE transactions on medical imaging*, vol. 34, no. 2, pp. 357–365, 2015.
- [26] H. Zamani, H. Zayyani, and F. Marvasti, "An iterative dictionary learning-based algorithm for doa estimation," *IEEE Communications Letters*, vol. 20, no. 9, pp. 1784–1787, 2016.
- [27] S. S. Sadrizadeh, S. Kiani, M. Boloursaz, and F. Marvasti, "Iterative method for simultaneous sparse approximation," *Scientia Iranica*, 2018.
- [28] A. Buades, B. Coll, and J.-M. Morel, "A non-local algorithm for image denoising," in *Computer Vision and Pattern Recognition, 2005. CVPR 2005. IEEE Computer Society Conference on*, vol. 2. IEEE, 2005, pp. 60–65.
- [29] K. He, J. Sun, and X. Tang, "Guided image filtering," *IEEE transactions on pattern analysis & machine intelligence*, no. 6, pp. 1397–1409, 2013.

- [30] H. R. Sheikh and A. C. Bovik, "Image information and visual quality," in *2004 IEEE International Conference on Acoustics, Speech, and Signal Processing*, vol. 3. IEEE, 2004, pp. iii–709.
- [31] L. Stanković and M. Brajović, "Analysis of the reconstruction of sparse signals in the dct domain applied to audio signals," *IEEE/ACM Transactions on Audio, Speech, and Language Processing*, vol. 26, no. 7, pp. 1220–1235, 2018.
- [32] M. Ciołek and M. Niedźwiecki, "Detection of impulsive disturbances in archive audio signals," in *2017 IEEE International Conference on Acoustics, Speech and Signal Processing (ICASSP)*. IEEE, 2017, pp. 671–675.
- [33] J. Nuzman, "Audio restoration: An investigation of digital methods for click removal and hiss reduction," *University of Maryland, Institute for Advanced Computer Studies*, 2004.
- [34] N. Ahmed, T. Natarajan, and K. R. Rao, "Discrete cosine transform," *IEEE transactions on Computers*, vol. 100, no. 1, pp. 90–93, 1974.